3b2 Version Number : 7.51c/W (Jun 11 2001)
File path : p:Santype/Journals/Taylor&Francis/Unht/v49n1/UNHT132483/UNHT132483.3d
Date and Time : 30/9/05 and 19:49

Numerical Heat Transfer, Part A, 49: 1–24, 2006

ISSN: 1040-7782 print/1521-0634 online
DOI: 10.1080/10407780500325001

FLOW AND HEAT TRANSFER IN A PARALLEL-PLATE CHANNEL WITH POROUS AND SOLID BAFFLES

Nicolau B. Santos and Marcelo J. S. de Lemos
Departamento de Energia—IEME, Instituto Tecnológico de Aeronáutica—ITA, São José dos Campos SP, Brazil

Simulations are presented for laminar flow in a channel containing baffles made with solid (impermeable) and porous materials. The equations of mass continuity, momentum and energy are written for an elementary representative volume, yielding a set of equations valid for the entire computational domain. These equations are discretized using the control-volume method and the resulting system of algebraic equations is relaxed with the SIMPLE method. The numerical results for the friction factor f and for the Nusselt number Nu are compared with available data, indicating that results herein differ by less than 5% in relation to published results. Further simulations comparing the effectiveness of the porous material used show that no advantages are obtained when using low-porosity baffles in the laminar flow regime investigated here.

1. INTRODUCTION

Flow and heat transfer in channels with solid or impermeable baffles have attracted attention of researchers due to the technological advantages in increasing energy transfer in engineering equipment [1–10]. If the baffles are made of a permeable or perforated material, flow head losses might be substantially reduced. Accordingly, due to the growing applicability of porous media in many fields of engineering and science, such as petroleum and gas engineering, heat exchangers, combustion in porous matrices, cooling of electronic devices, to mention only a few, a good understanding of transport processes in such media is of advantage to the design and analysis of engineering equipment.

Berner et al. [1] presented the main features of the flow in a channel with solid baffles (Figure 1*a*). This was obtained using flow visualization techniques, manometry, and laser Doppler anemometry. The experiment was applied to a two-dimensional water flow around baffles, with $L/H = 1$, h/H from 0.5 to 0.9, and Reynolds number Re ranging from 600 to 10,500. They suggested that laminar flow occurred for $\mathrm{Re} \leq 600$. Following the work in [1], Kelkar and Patankar [2] presented numerical simulations for laminar flow in a channel with solid baffles for Re ranging from 100 to 500. They concluded that for high Prandtl number fluids, heat

Received 27 April 2005; accepted 15 July 2005.
The authors would like to thank CNPq and FAPESP, Brazil, for their invaluable financial support during the course of this research.
Address correspondence to Marcelo J. S. de Lemos, Departamento de Energia—IEME, Instituto Tecnológico de Aeronáutica—ITA, 12228-900 São José dos Campos SP, Brazil. E-mail: delemos@ita.br

NOMENCLATURE

c_F	Forchheimer coefficient (=0.55)
f	friction factor
h	baffle height (=20 mm)
H	channel height (=40 mm)
K	permeability
k_f	fluid thermal conductivity
k_s	solid thermal conductivity
L	cell length (=H=40 mm)
L_c	test section length (=600 mm)
L_i	entry length (=400 mm)
L_t	channel length (=1,400 mm)
Nu	Nusselt number
$\langle \bar{p} \rangle^i$	intrinsic average pressure
Pr	Prantdl number
Re	Reynolds number ($= 2H\rho \mathbf{u}_D^*/\mu$)
Q_{cell}	heat transferred to a single cell
t	baffle thickness (=1.5 mm)
T_b	bulk temperature
T_f	fluid temperature
T_s	solid temperature
$\mathbf{u}_D$	local surface velocity
$\mathbf{u}_D^*$	average surface velocity $\left(= \frac{1}{H}\int_0^H \mathbf{u}_D \, dy\right)$
δ	coefficient for grid influence on friction factor $\left[= \left(\frac{f\|_{\text{ref}} - f}{f\|_{\text{ref}}}\right) \times 100\right]$
ε	coefficient for grid influence on Nusselt number $\left[= \left(\frac{\overline{\text{Nu}}\|_{\text{ref}} - \overline{\text{Nu}}}{\overline{\text{Nu}}\|_{\text{ref}}}\right) \times 100\right]$
η	coefficient for heat transfer comparison $\left[= \frac{\overline{\text{Nu}^*}\|_{\text{porous}} - \overline{\text{Nu}^*}\|_{\text{solid}}}{\overline{\text{Nu}^*}\|_{\text{solid}}} \times 100\right]$
λ	fin-conductance parameter $[=k_s t/(k_f L)]$
μ	fluid molecular viscosity
ρ	fluid density
ϕ	porosity
ψ_0	maximum value of normalized stream function in the main recirculating eddy

Subscripts

b	bulk
D	Darcy
f	fluid
ref	reference
s	solid
0	parallel-plate channel

transfer within the channel is significantly enhanced, a result that is in agreement with similar predictions by Webb and Ramadhyani [3]. Lopez et al. [4] investigated three-dimensional effects for this same geometry and obtained similar results as those taken at the center of the channel. Further, Huang and Vafai (1994) [5] studied heat transfer enhancement in channels containing porous cavities and block obstacles.

The first experimental work investigating the use of permeable baffles, instead of using solid plates, was presented by Hwang [6]. In that work, the author found out that heat transfer between the channel walls and the fins was enhanced, showing then that for turbulent flow the use of porous baffles benefited heat transfer, i.e., the use of porous baffles in substitution to solid (impermeable) material represented a net gain. Motivated by this article, Yang and Hwang [7] carried out a numerical investigation of the problem, reaching similar conclusions. To corroborate Hwang's [6] conclusion, Ko and Anand [8] carried out an experimental program for turbulent flow with porous baffles made of various materials. However, results in [8] were not very promising. In their analysis, the porous baffles presented in most cases a flow behavior as good as the one with solid baffles. Da Silva Miranda and Anand [9] presented a numerical analysis of laminar air flow in a channel with porous baffles having height $h/H = 0.33$, thickness t/H from 0.09 to 0.25, permeability K from 10^{-7} to $7.6 \times 10^{-8}\,\text{m}^2$, porosity $\phi = 0.92$, and $\lambda = k_s t/(k_f L)$ ranging from 0.09 to 330. More recently, Haji-Sheikh et al. [10] published a detailed numerical study of heat transfer to a fluid in a saturated porous medium using the Green's function method.

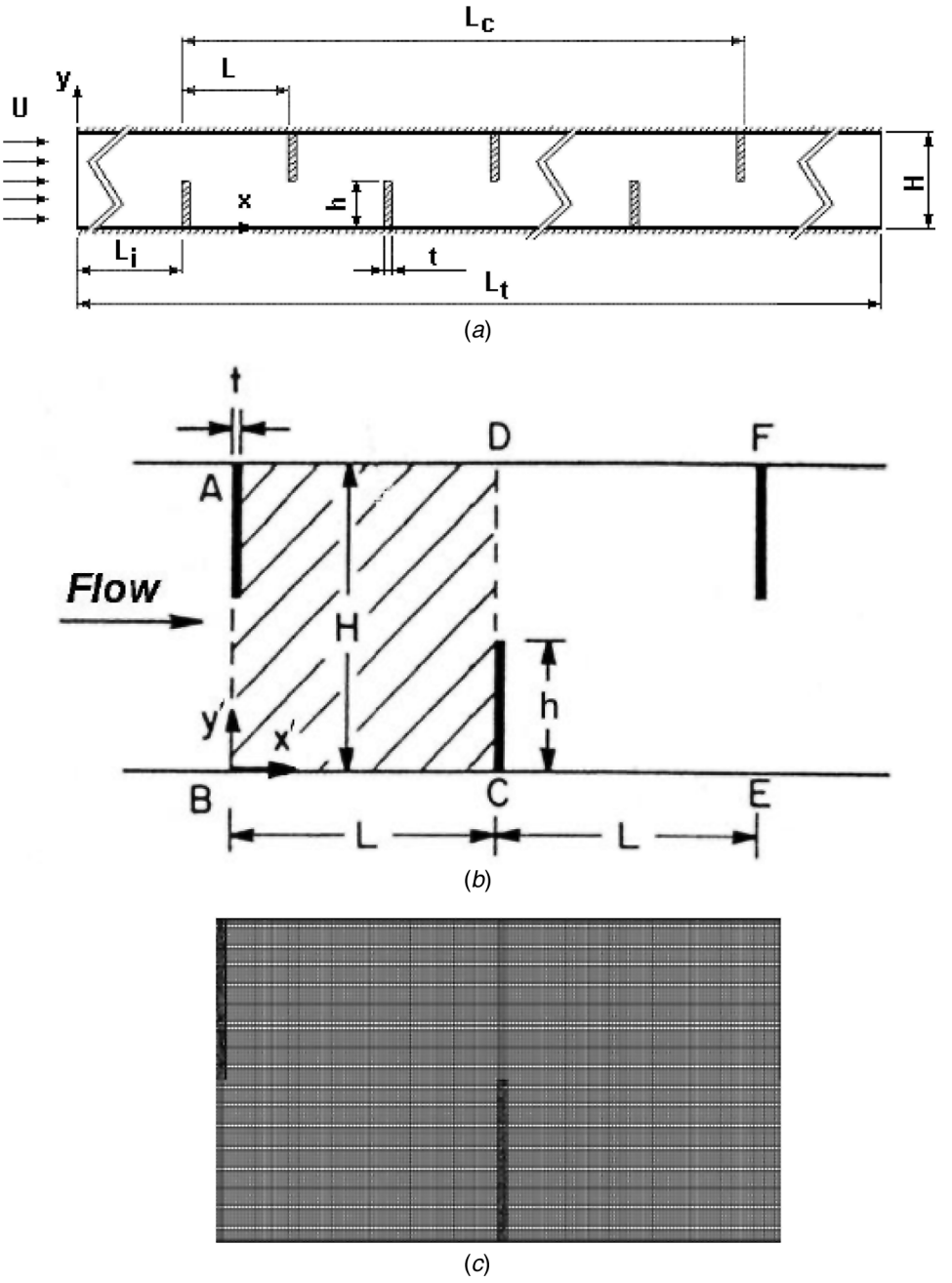

Figure 1. Problem under consideration: (*a*) geometry; (*b*) channel cell; (*c*) section of computational grid of length $2L$.

In summary, references [8, 9] noticed that in none of the cases analyzed (with the substitution of the solid baffles for porous baffles) was an increase in the overall heat transfer along the channel obtained.

Motivated by such engineering application, Rocamora and de Lemos [11, 12] presented numerical solutions for laminar flow in hybrid (clear/porous) media. One of the greatest difficulties in numerically solving such hybrid systems arises in the treatment given at the interface between the two media. Most models consider constant properties for the porous substrate, but, close to the interface, the permeability of the medium is known to increase. This effect is commonly modeled by a difference in the macroscopic shear stress at both sides of the macroscopic interface. Therefore, due to the importance of this particular theme, a literature review on this subject is also briefly included here. In fact, Rocamora and de Lemos [11, 12] did not consider a stress jump at the interface between the porous medium and the clear fluid. In the literature, for laminar flow, Ochoa-Tapia and Whitaker [13, 14] proposed an adjustable coefficient for modeling the stress jump at the interface. Kuznetsov [15–17] presented analytical solutions for laminar velocity profiles in a channel partially filled with porous material, taking into consideration such a jump condition. Turbulent flow in a parallel-plate composite channel has also been investigated [18]. Recently, Silva and de Lemos [19] presented numerical solutions for this same geometry, also considering the jump at the interface.

Tofaneli and de Lemos [20] investigated isothermal laminar flow in a channel containing porous fins. The channel, shown schematically in Figure 1*a*, had baffles made of porous and solid material attached to both walls. In that work, the effects of inlet Reynolds number and jump coefficients were considered and use was made of the numerical methodology proposed in Silva and de Lemos [19]. Later, Tofaneli and de Lemos [21] investigated the influence of porosity and permeability on the flow pattern in the same geometry (Figure 1*a*). Subsequently, de Lemos and Tofaneli [22, 23] further extended the earlier results of Tofaneli and de Lemos [20, 21], comparing the pressure drop for turbulent flow along the channel of Figure 1. The macroscopic mathematical model used in [20, 21] has been developed by de Lemos and co-workers [24–42]. That development is based on the recently proposed double-decomposition concept, which considers time fluctuations and spatial deviations of all variables in a porous medium. Such a model, which was initially proposed for the flow variables [24–28], has been extended to heat transfer in porous media [29–30]. Further, a consistent program of systematic studies based on the double-decomposition theory for treating turbulence in porous media including buoyant flows [31–33], mass transfer [34], nonequilibrium heat transfer [35], double diffusion [36], and hybrid media (clear/porous domains) [37–41], in addition to a general classification of models [42], is available in the open literature.

Following up with the work in baffled channels, Santos and de Lemos [43] and de Lemos and Santos [44] carried out a numerical analysis of the flow with heat transfer in a parallel-plate channel containing 16 porous baffles made with material having permeability $K = 10^{-9}$ m^2 and porosity $\phi = 0.4$. Their results indicated that, in spite of using a permeable medium, total drag and heat transfer along the channel were close to those obtained with solid plates, possibly due to the extremely low permeability used. Santos and de Lemos [45] further investigated the influence of permeability and porosity on flow and heat transfer in a porous baffled channel with

$h/H = 0.5$, $\mathrm{Pr} = 0.7$, and $\lambda = 0.4$. They concluded that there was not an effective increase in heat transfer when porous baffles were used.

The purpose of the present contribution is to investigate and document a numerical analysis on flow and heat transfer along a channel with porous and solid baffles. The influence of the permeability and porosity of the material is analyzed, in addition to the effect of the fluid properties ($0.7 < \mathrm{Pr} < 7.0$), baffle material ($0.04 < \lambda < 40$), and geometry ($0.25 < h/H < 0.75$). Here, only one unique set of transport equations is used for both the clear domain and the porous medium.

2. MATHEMATICAL MODEL

The mathematical model employed here has its origin in the works of Pedras and de Lemos [24–28]. The numerical implementation of the jump condition at the interface was considered by Silva and de Lemos [19] based on the theory proposed by Ochoa-Tapia and Whitaker [13, 14]. Nevertheless, for the sake of simplicity, in this work no jump condition was considered. Therefore governing equations, in their laminar model form, will be just reproduced here and details about their derivations can be obtained in the mentioned articles. These equations are as follows.

Macroscopic continuity equation:

$$\nabla \cdot \mathbf{u}_D = 0 \tag{1}$$

where $\mathbf{u}_D$ is the average surface velocity (also known as seepage, superficial, filter, or Darcy velocity). Equation (1) represents the macroscopic continuity equation for an incompressible fluid.

Macroscopic momentum equation:

$$\rho\nabla \cdot \frac{\mathbf{u}_D\mathbf{u}_D}{\phi} = -\nabla\phi\langle p\rangle^i + \mu\nabla^2\mathbf{u}_D - \left(\frac{\mu\phi}{K}\mathbf{u}_D + \frac{c_F\phi\rho}{\sqrt{K}}|\mathbf{u}_D|\mathbf{u}_D\right) \tag{2}$$

where the last two terms in Eq. (2) represent the Darcy-Forchheimer contribution. The symbol K is the porous medium permeability, $c_F = 0.55$ is the form drag coefficient (Forchheimer coefficient), $\langle p\rangle^i$ is the intrinsic (volume-averaged on fluid phase) pressure of the fluid, ρ is the fluid density, μ represents the fluid viscosity, and ϕ is the porosity of the porous medium.

Macroscopic energy equation:

$$\begin{aligned}\left(\rho c_p\right)_f\nabla \cdot \left(\mathbf{u}_D\langle T\rangle^i\right) &= \nabla \cdot \left\{\left[k_f\phi + k_s(1-\phi)\right]\nabla\langle T\rangle^i\right\} \\ &\quad + \nabla \cdot \left[\frac{1}{\Delta V}\int_{A_i}\mathbf{n}\left(k_fT_f - k_sT_s\right)dS\right] \\ &\quad - \left(\rho c_p\right)_f\nabla \cdot \left[\phi\left(\left\langle {}^i\mathbf{u}^iT_f\right\rangle^i\right)\right]\end{aligned} \tag{3}$$

where T_f and T_s are the local fluid and solid temperatures, respectively, and k_f and k_s are the thermal conductivities for the fluid and for the solid. Further, the homogenous model assumes that intrinsic (phase-averaged) temperatures for the solid and for the fluid are equal, or $\langle T_s \rangle^i = \langle T_f \rangle^i = \langle T \rangle^i$.

At the interface, the conditions of continuity of velocity, pressure, and temperature read

$$\mathbf{u}_D|_{0<\phi<1} = \mathbf{u}_D|_{\phi=1} \tag{4}$$

$$\langle p \rangle^i|_{0<\phi<1} = \langle p \rangle^i|_{\phi=1} \tag{5}$$

$$\langle T \rangle^i|_{0<\phi<1} = \langle T \rangle^i|_{\phi=1} \tag{6}$$

The nonslip condition for velocity is applied on both walls.

3. NUMERICAL METHOD AND COMPUTATIONAL DETAILS

The numerical method utilized to solve the flow equations is the finite-volume method applied to a boundary-fitted coordinate system. Equations (1)–(3) subjected to boundary and interface conditions Eqs. (4)–(6), were discretized in a two-dimensional control volume involving both clear and porous media. The numerical method used in the resolution of the equations above was the SIMPLE algorithm, as described by Patankar [46]. The interface is positioned to coincide with the border between two control volumes, generating, in such a way, only volumes of the types "totally porous" or "totally clear." The flow equations are then resolved in the porous and clear domains, considering the interface conditions mentioned earlier. Details of the numerical implementation can be seen in Silva and de Lemos [19].

3.1. Friction Factor

The friction factor in a section of the channel, shown in Figure 1*b*, can be calculated as

$$f = \frac{\Delta P}{\rho} \frac{D_h}{L} \frac{2}{\overline{U}^2} \tag{7}$$

where ΔP is the pressure loss for the cell, $\overline{U}$ is the mean velocity, and $D_h = 2H$ is the hydraulic diameter. Also, for flow between infinite parallel plates without baffles, the friction factor is given by

$$(f \, \mathrm{Re})_0 = 96$$

where the subscript 0 identifies values for unobstructed channels and the Reynolds number is defined as $\mathrm{Re} = \rho \overline{U} D_h / \mu$.

3.2. Nusselt Number

Heat transfer between the channel walls and the fluid, in the cell shown in Figure 1*b*, is calculated numerically using the Nusselt number defined by

$$\overline{\mathrm{Nu}} = \frac{\overline{h} D_h}{k_f} \tag{8}$$

where

$$\overline{h} = \frac{Q_{\mathrm{cell}}}{(2L \times 1)\Delta T_{ml}} \tag{9}$$

$$Q_{\mathrm{cell}} = \rho \overline{U} c_p (H \times 1)[T_b(0) - T_b(L)] \tag{10}$$

$$\Delta T_{ml} = \frac{[T_w - T_b(L)] - [T_w - T_b(0)]}{\ln\{[T_w - T_b(L)]/[T_w - T_b(0)]\}} \tag{11}$$

$$T_b(x') = \frac{\int_0^H uT\, dy'}{\int_0^H u\, dy'} \tag{12}$$

This formulation takes into consideration the heat transferred to the fluid, Q_{cell}, through the surfaces at a constant temperature, T_w, and the energy absorbed by the fluid via variation of bulk temperature along the cell, T_b. In this study, the channel wall temperature, T_w, is kept constant so that the definitions above apply.

4. RESULTS AND DISCUSSION

Before proceeding, a word about the nomenclature, simulating conditions, and grid size here employed seems timely.

In the context herein, the expression *solid baffle* means a structure through which no fluid permeates. On the other hand, *porous baffles* are here characterized by a solid matrix, not fully compacted, so that fluid can flow freely within the existing void space. In addition, all results in the figures are divided by corresponding values obtained in channels without baffles, which are here identified by subscript 0.

Further, only steady-state solutions are sought herein, and no consideration for unsteady or transient behavior is made. Accordingly, for the Re range here considered, most numerical results found in the literature discard the appearance of unsteady vortex motion.

Different grid sizes were employed in order to check their influence on the numerical values of f and Nu calculated in a fully developed channel cell, which is shown schematically in Figure 1*b*. Table 1 shows the percent errors δ and ε, defined as

$$\delta = \left(\frac{f|_{\mathrm{ref}} - f}{f|_{\mathrm{ref}}} \right) \times 100 \tag{13}$$

Table 1. Grid independence study

x	y	$f\ \mathrm{Re}/(f\ \mathrm{Re})_0$	$\overline{\mathrm{Nu}}/\overline{\mathrm{Nu}}_0$	δ	ε
952	62	150.5	4.61	18.7%	–2.4%
1,207	62	158.0	4.74	14.7%	−5.3%
1,357	62	160.2	4.77	13.5%	−6.0%
1,507	82	167.6	4.69	9.5%	−4.2%
1,507	122	173.0	4.59	6.6%	−2.0%
1,507	202	178.7	4.51	3.5%	−0.2%
1,507	302	177.7	4.48	4.0%	0.4%
2,112	302	185.2	4.50	ref	ref

and

$$\varepsilon = \left(\frac{\overline{\mathrm{Nu}}|_{\mathrm{ref}} - \overline{\mathrm{Nu}}}{\overline{\mathrm{Nu}}|_{\mathrm{ref}}} \right) \times 100 \tag{14}$$

for grids of several sizes, taken as reference calculations run on a $2{,}112 \times 302$ "ref" grid. The table indicates that for a grid of size $1{,}507 \times 202$, more economical solutions could be obtained while retaining accuracy and solution precision. All computations below were then obtained with such a grid, which is illustrated in Figure 1*c*.

4.1. Developing Flow

Developing profiles for f and Nu along the channel are shown in Figure 2 for solid baffles and in Figure 3 for porous fins. These numerical values for ϕ and K used in Figure 3 correspond to those used in the literature [4, 6–8]. One can see in the figures that fully developed flow and heat transfer are obtained only after the 11th cell. Therefore, comparison of overall head losses and heat transfer characteristics will use values calculated past that particular axial position. It can also be seen that, although porous baffles were used for comparison with the solid cases, their values for K and ϕ were such that no significant difference appears to exist between both situations. Therefore, shown below are the results past the 11th cell, which are compared with those by Kelkar and Patankar [2] and Lopez et al. [4].

4.2. Fully Developed Flow

4.2.1. Streamlines Figure 4 shows comparisons of calculated streamlines with those presented by Kelkar and Patankar [2] for solid baffles. Also shown in the figure are results for porous baffles. One can see that the present results (*b*) reproduce well literature data for solid-baffle cases (*a*). For porous baffles with $K = 1 \times 10^{-9}\,\mathrm{m}^2$ and $\phi = 0.4$, it is noticeable that the recirculation strength ψ_0 is slightly reduced (*c*). The numerical parameter ψ_0 was introduced by Kelkar and Patankar [2] and represents a relation between the maximum recirculation rate within the cell and the mass flow rate through the channel. Also observed in the figure is the detachment of streamlines from the porous baffle since the no-slip condition, prevailing over a solid surface, is no longer applicable when a permeable baffle is considered.

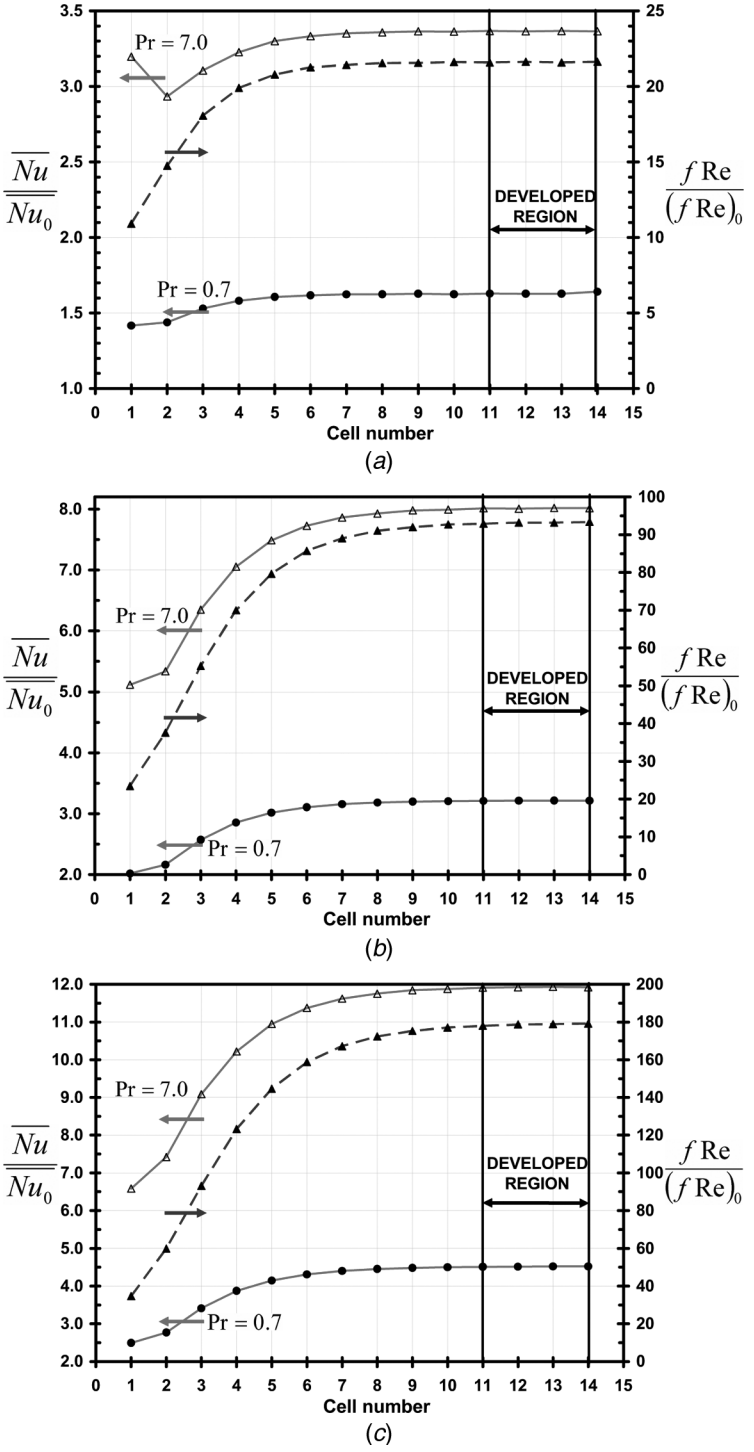

Figure 2. Developing Nu and f for a channel with solid baffles, $h/H = 0.5$, $\lambda = 0.4$: (*a*) Re = 100; (*b*) Re = 300; (*c*) Re = 500.

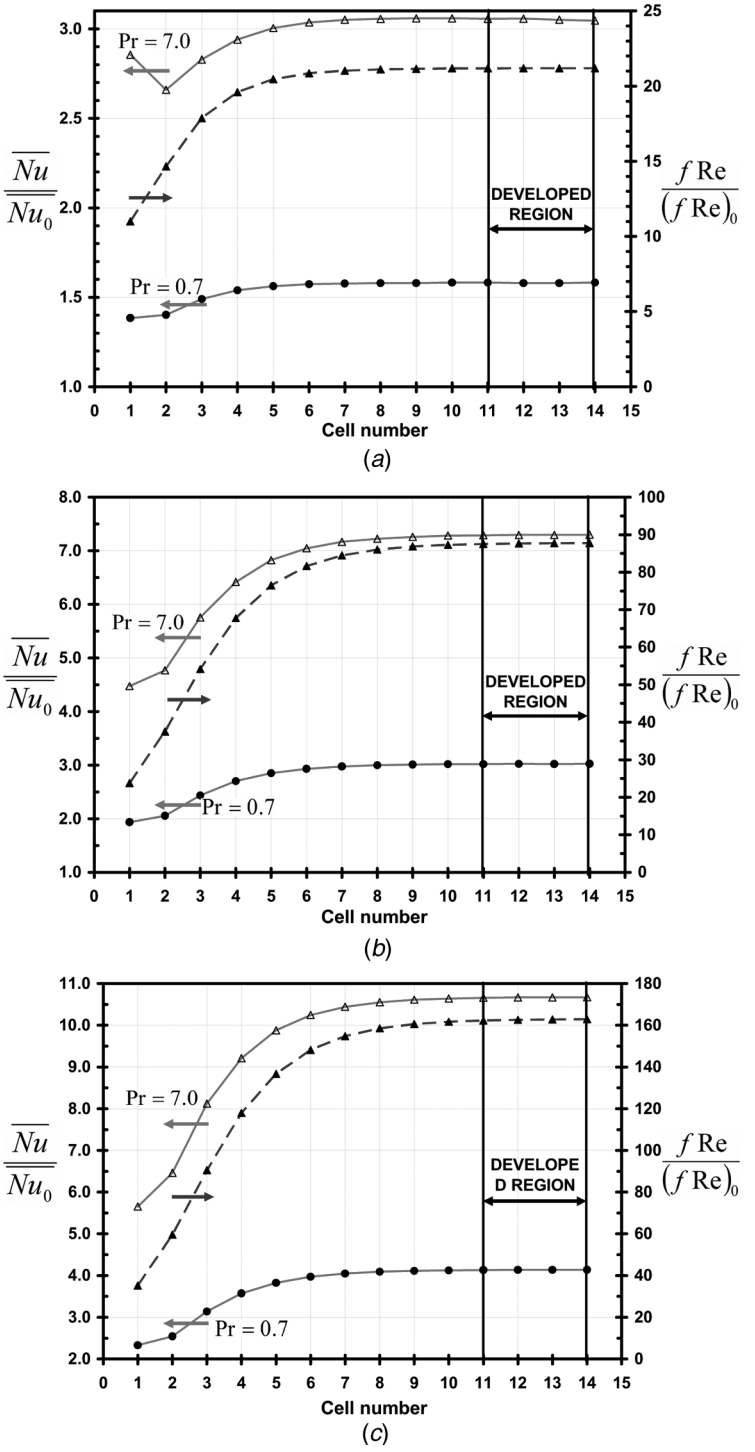

Figure 3. Developing Nu and f for a channel with porous baffles, $h/H = 0.5$, $K = 1 \times 10^{-9}$ m^2, $\phi = 0.4$, $\lambda = 0.4$: (*a*) Re = 100; (*b*) Re = 300; (*c*) Re = 500.

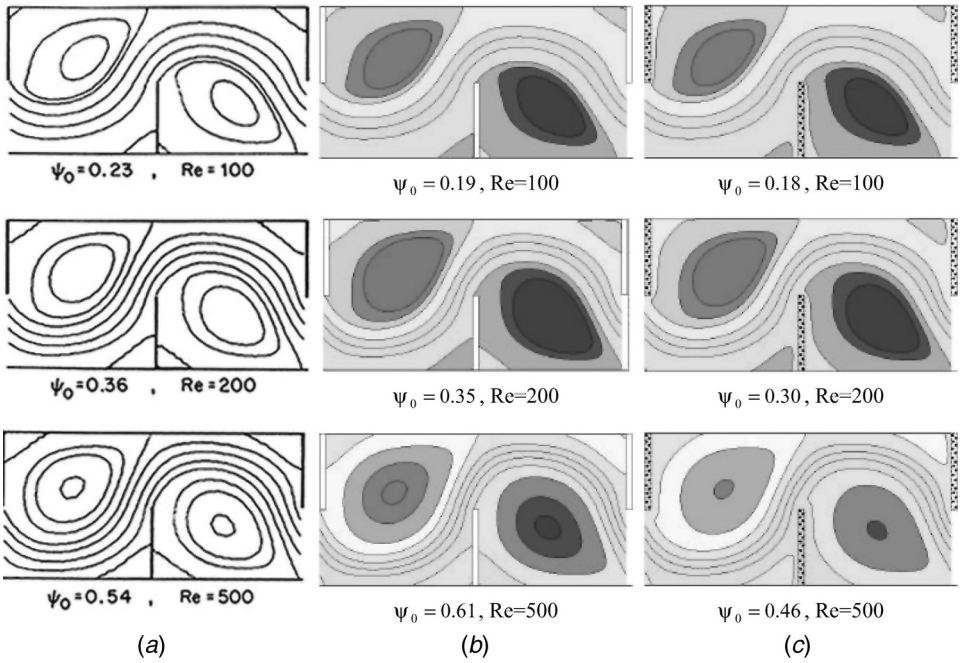

Figure 4. Streamlines pattern as a function of Re for $h/H = 0.5$: (*a*) solid baffles, Kelkar and Patankar [2]; (*b*) present work, solid baffles; (*c*) present work, porous baffles, $K = 1 \times 10^{-9}\,\mathrm{m}^2$, $\phi = 0.4$.

Figure 5 presents the influence of the baffle height h/H on the stream function pattern, indicating that, as expected, ψ_0 increases when h/H rises, for both porous and solid baffles. Higher baffles, of either porous or solid type, retain more fluid within the recirculating bubbles.

Figure 6 shows the effect of permeability K on the flow pattern, for different values of Re. It can seen that the cell recirculating strength ψ_0 decreases as K increases, and essentially vanishes for $K = 10^{-7}\,\mathrm{m}^2$. It is interesting to observe the opposing effect of Re on the recirculating mass flow rate in the cell for different K values. In Figure 6*a*, for a less permeable baffle ($K = 10^{-9}\,\mathrm{m}^2$), an increase in Re increases ψ_0, whereas for a more permeable medium (Figure 6*b*, $K = 1 \times 10^{-8}\,\mathrm{m}^2$), more flow is ''pushed'' through the cell as the channel mass flow rate increases (lower ψ_0). The effect of porosity ϕ is presented in Figure 7, but as one can see, porosity does affect flow parameters as substantially as the permeability does.

4.2.2. Friction factor The effect of Re on fully developed values of f is shown in Figure 8*a*, where the present results are compared with similar data from the literature. The curves reflect the rise in the f value in relation to an unobstructed channel flow (''0'' conditions). Results compare well with publish data indicating an increase in f as the mass flow rate through the channel is increased. The effect of permeability K on friction factor f is presented in Figure 8*b*. Results show that porous baffles of any type will always yield smaller friction factors and that a decrease in f is observed for higher permeabilities. Also show in Figure 8*b* is the slight reduction on f for a more porous material (higher ϕ). Less sensitivity of flow

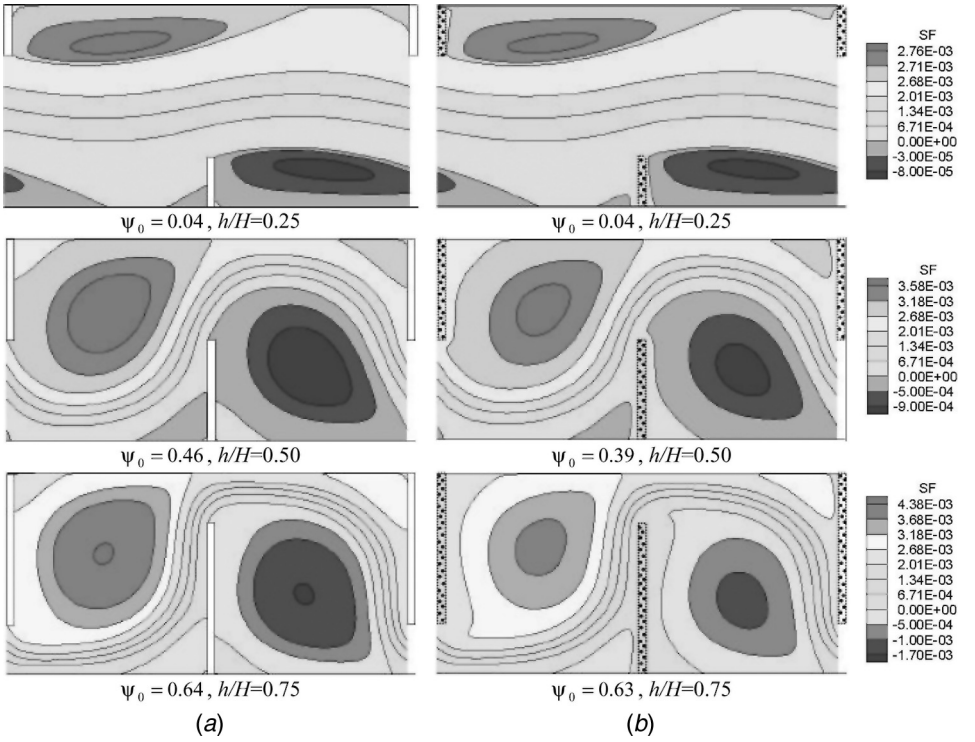

Figure 5. Streamlines pattern as a function of h/H, $\mathrm{Re} = 300$: (*a*) solid baffles; (*b*) porous baffles, $K = 1 \times 10^{-9}\,\mathrm{m}^2$, $\phi = 0.4$.

parameters on variations in ϕ is also seen in Figure 9*a*, where for a wide range of porosities no substantial change in f is detected. The influence of baffle height is presented in Figure 9*b*, where it is noticed that the head loss increases significantly with greater h/H values. Also, it is noted that when a porous baffle is employed, the higher the baffle height, the bigger is the difference between the solid and the porous cases.

4.2.3. Nusselt number Figure 10*a* presents results for Nu as a function of Re and solid material properties. The coefficient λ is defined as

$$\lambda = \frac{k_s}{k_f}\frac{t}{L} \tag{15}$$

Results in the figure compare well with published data and reproduce the enhancement on the heat transfer characteristics as the solid conductivity or the fluid Pr number increases. Figure 10*b* shows the reduction in Nu for more permeable baffles, in coherence with reduction of recrculating strengths shown in Figure 6 and consequent lower drag in Figure 8. The effect on conductivity ratio is presented in Figure 10*c*, where an increase in Nu with higher λ is observed. Also, porosity affects

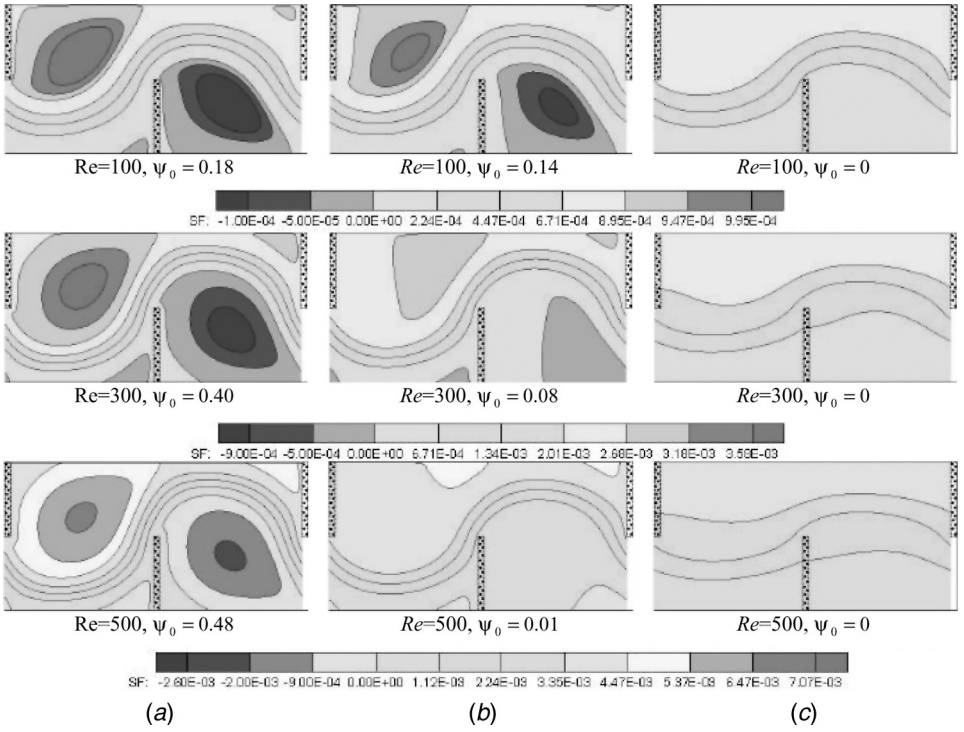

Figure 6. Streamlines pattern as a function of K for $h/H = 0.5$ and $\phi = 0.9$: (*a*) $K = 1 \times 10^{-9}\,\mathrm{m}^2$; (*b*) $K = 1 \times 10^{-8}\,\mathrm{m}^2$; (*c*) $K = 1 \times 10^{-7}\,\mathrm{m}^2$.

heat transfer more efficiently for materials with high thermal conductivity. In Figure 10*c* the Nu values for $\phi = 0.4$ are higher than those of $\phi = 0.9$ when λ is equal to 40.

Figure 11*a* shows a reduction in Nu in relation to the solid-baffle case when a highly impermeable (compacted) material is used for manufacturing porous baffles. The influence of λ on Nu is presented in Figure 11*b* for two Prandtl numbers. For the conditions used, Nu increases with both Pr and λ and is slightly higher for the solid-baffle case. As in the case of f (Figure 9*a*), Nu is also less sensitive to ϕ, as seen in Figure 12*a*. Further, the channel height affects Nu (Figure 12*b*) as if affects f (Figure 9*b*), essentially by enhancing ψ_0 within the channel cell (see Figure 5).

4.2.4. Effective heat transfer For analyzing the effective influence of the type of obstruction (solid or porous), a modified Nusselt number $\overline{\mathrm{Nu}}^* = \left(\overline{\mathrm{Nu}}/\overline{\mathrm{Nu}_0}\right)/(f/f_0)^{1/3}$ has been proposed in the literature (Ko and Anand [8]). This modified Nusslet number is a measure of the head loss, when a porous medium is used, with the corresponding reduction in the heat transfer characteristics. Such analysis is useful when comparing performances of baffles of different types. Ultimately, if using porous baffles increases the value of $\overline{\mathrm{Nu}}^*$, in relation to using solid material, then the system is considered to be more effective. In this case, although Nu is reduced, the corresponding decrease in the necessary pumping power (reduction of f) makes it advantageous to use permeable material for manufacturing the baffles (see [8] for details).

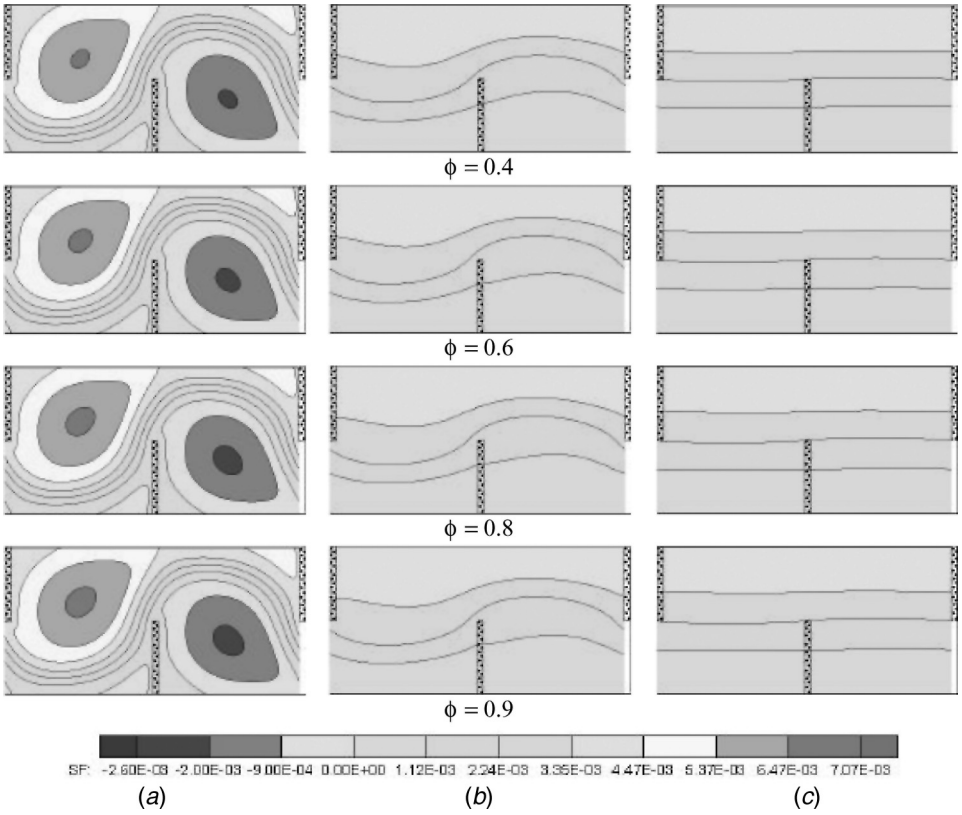

Figure 7. Streamlines as a function of ϕ, Re = 500, $h/H = 0.5$: (*a*) $K = 1 \times 10^{-9}\,\mathrm{m}^2$; (*b*) $K = 1 \times 10^{-7}\,\mathrm{m}^2$; (*c*) $K = 1 \times 10^{-5}\,\mathrm{m}^2$.

Table 2 presents values for $\overline{\mathrm{Nu}}^*$ and compares, for different Re and Pr, the effectiveness of both impermeable (solid) and porous baffled channels. The percent deviation, η, between these two values is also shown in the table and is calculated as

$$\eta = \frac{\overline{\mathrm{Nu}}^*\big|_{\mathrm{porous}} - \overline{\mathrm{Nu}}^*\big|_{\mathrm{solid}}}{\overline{\mathrm{Nu}}^*\big|_{\mathrm{solid}}} \times 100 \tag{16}$$

A positive value for η would indicate an enhancement in the effective heat transfer when using porous materials. However, the table shows that, for the porous material employed here and for the flow regime simulated here, no gain is obtained as far as heat transfer is concerned. Also noticed are more degraded conditions for the case of a higher Prandtl number.

Table 3 presents the influence of baffle height h/H on $\overline{\mathrm{Nu}}^*$ and η. The table shows that the use of shorter baffles is more advantageous for increasing heat transfer characteristics of this thermal equipment. This is related to a less significant head loss in porous material for low values of h/H, as indicated in Figure 9*b*.

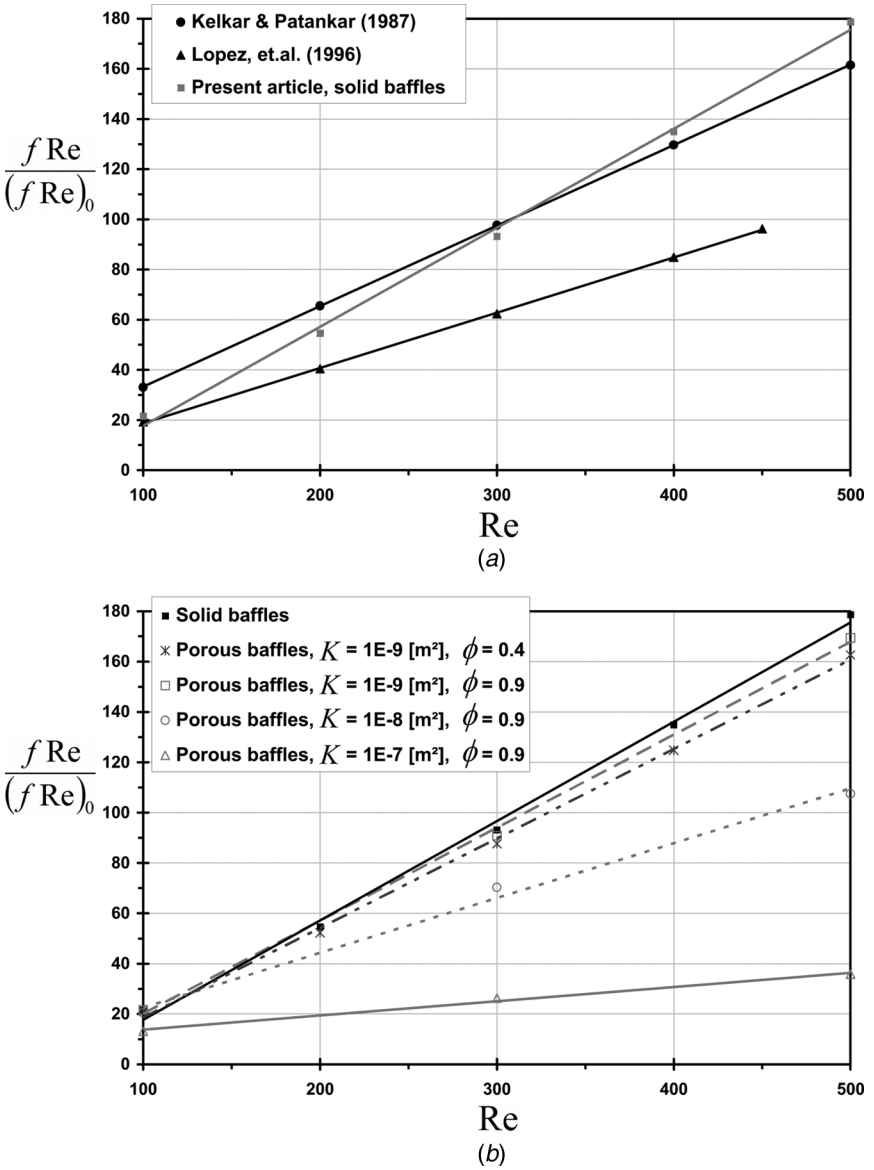

Figure 8. Friction factor for a channel as a function of Re, $h/H = 0.5$: (*a*) solid baffles; (*b*) porous baffles.

Here, when comparing the corresponding performance of porous and solid baffles under the same conditions, i.e., the same Re, Pr, K, and h/H, the use of the parameter λ, previously proposed in [2], was adopted. This parameter was 295
defined in [2] for analyzing the performance of solid baffles and did not consider the effective conductivity of the porous material due to the porosity. Accordingly, for a fixed λ, variation of ϕ indicates how the amount of solid material in the porous baffle affects heat transfer characteristics. On the other hand, calculations for a

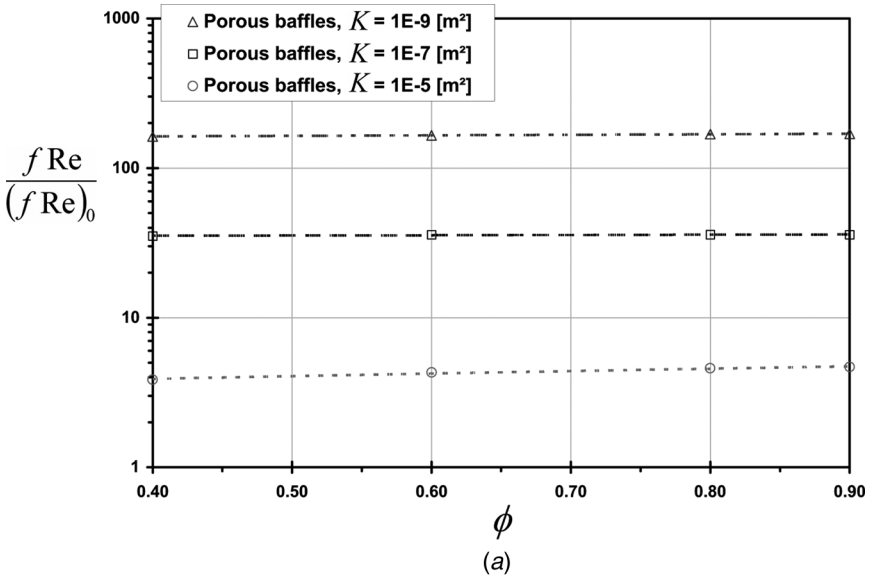

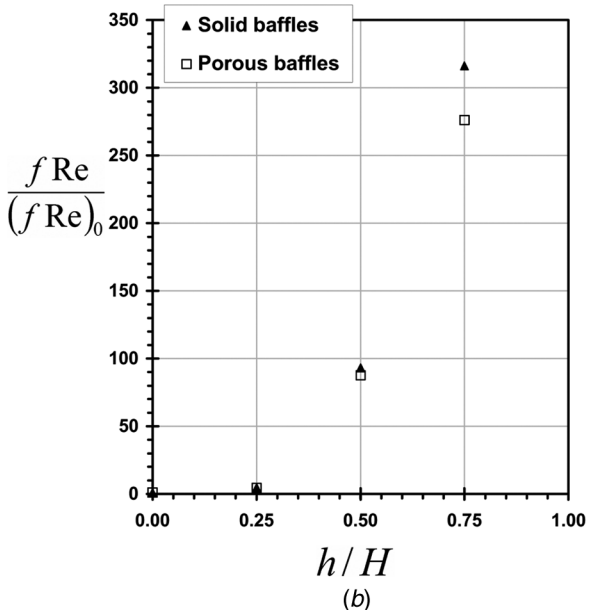

Figure 9. Friction factor for a channel with baffles: (*a*) effect of ϕ, $h/H = 0.5$; (*b*) effect of h/H, $K = 1 \times 10^{-9}\,\mathrm{m}^2$ and $\phi = 0.4$.

constant porosity ϕ, using distinct values of λ, reveal the influence of thermal conductivity of the solid material. 300

In Table 4, the effect of the solid thermal conductivity k_s (or λ) and Prandtl number on $\overline{\mathrm{Nu}}^*$ is evaluated for baffles with $\phi = 0.40$ and $h/H = 0.5$. It is possible to verify that an increase in λ (or k_s) results in an increase in $\overline{\mathrm{Nu}}^*$, regardless of the Pr

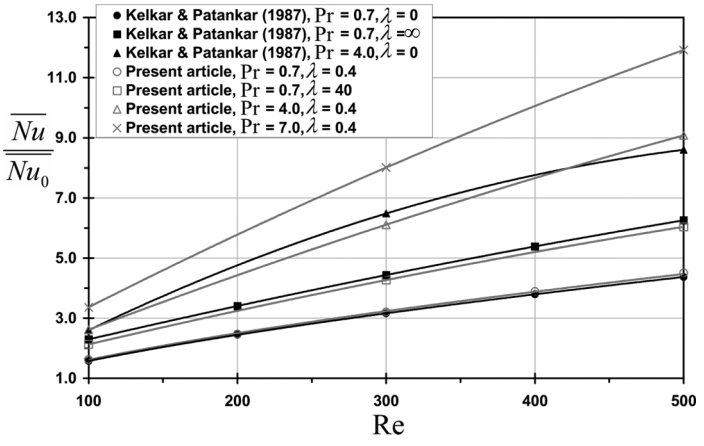

(*a*)

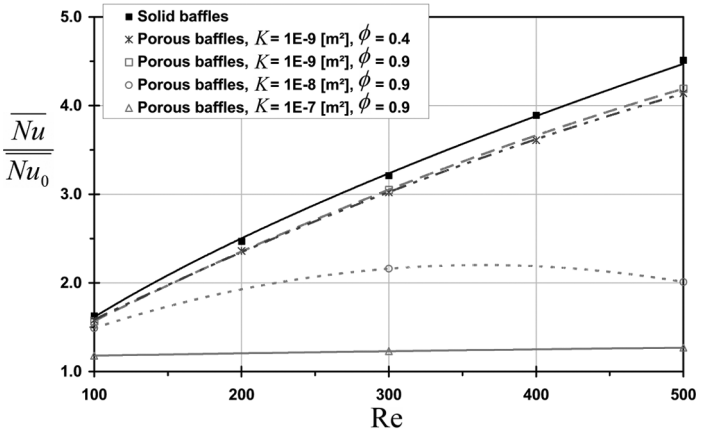

(*b*)

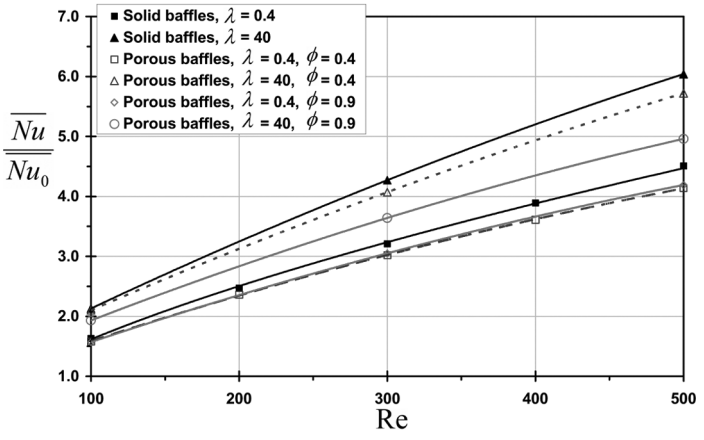

(*c*)

Figure 10. Nusselt number for a channel as a function of Re, $h/H = 0.5$: (*a*) solid baffles; (*b*) effect of K and ϕ, $\lambda = 0.4$, $\mathrm{Pr} = 0.7$; (*c*) effect of λ and ϕ, $K = 1 \times 10^{-9}\ \mathrm{m}^2$, $\mathrm{Pr} = 0.7$.

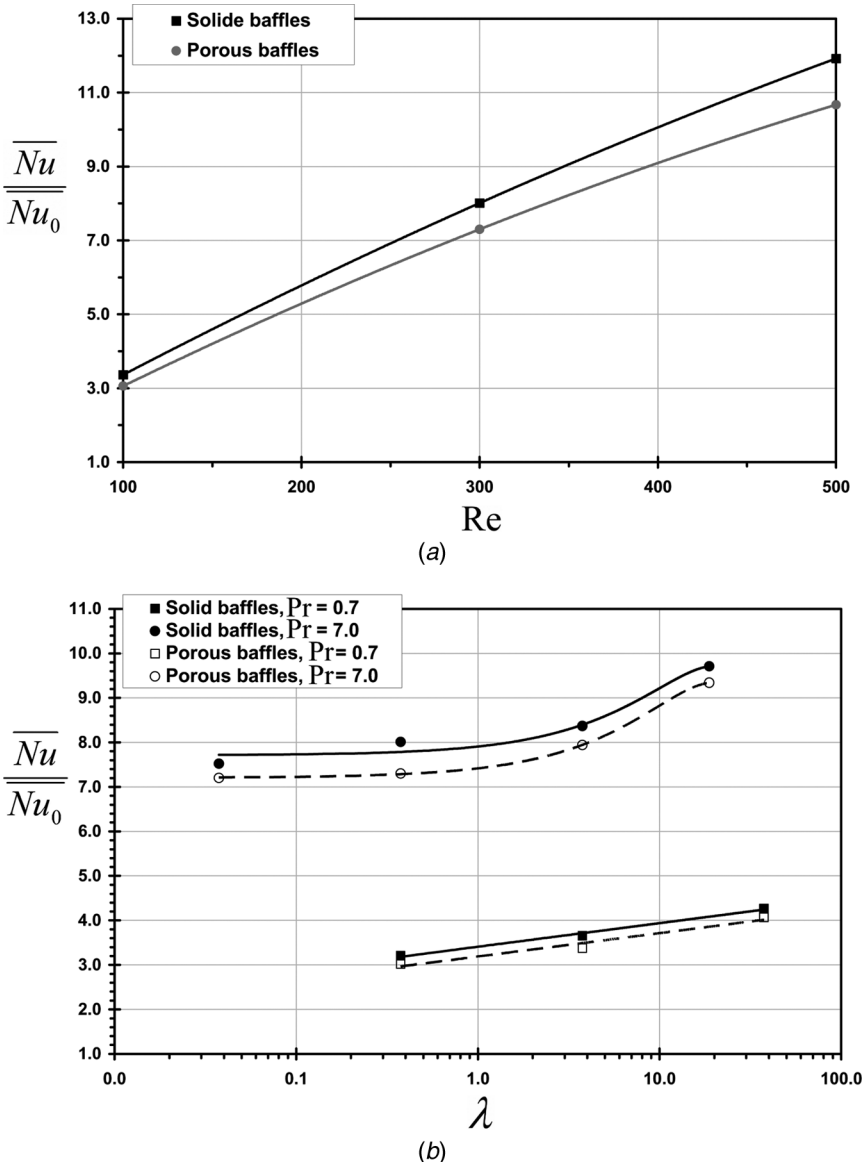

Figure 11. Nusselt number for a channel with solid and porous baffles, $h/H = 0.5$, $K = 1 \times 10^{-9}\,\mathrm{m}^2$; $\phi = 0.4$: (*a*) effect of Re, Pr = 7.0, and $\lambda = 0.4$; (*b*) effect of λ.

used. The table also indicates that optimal values for η will depend on a combination of the solid material (λ) and the working fluid (Pr) used. Table 5 shows the effect of porosity ϕ on $\overline{\mathrm{Nu}}^*$ for different Re and λ. Only for larger values of λ is a reduction in $\overline{\mathrm{Nu}}^*$ observe as ϕ increases. Porous baffles made of highly conductivity material ($\lambda = 40$) and of relatively low porosity ($\phi = 0.4$) present the best advantages (higher η) over the range of Re investigated here.

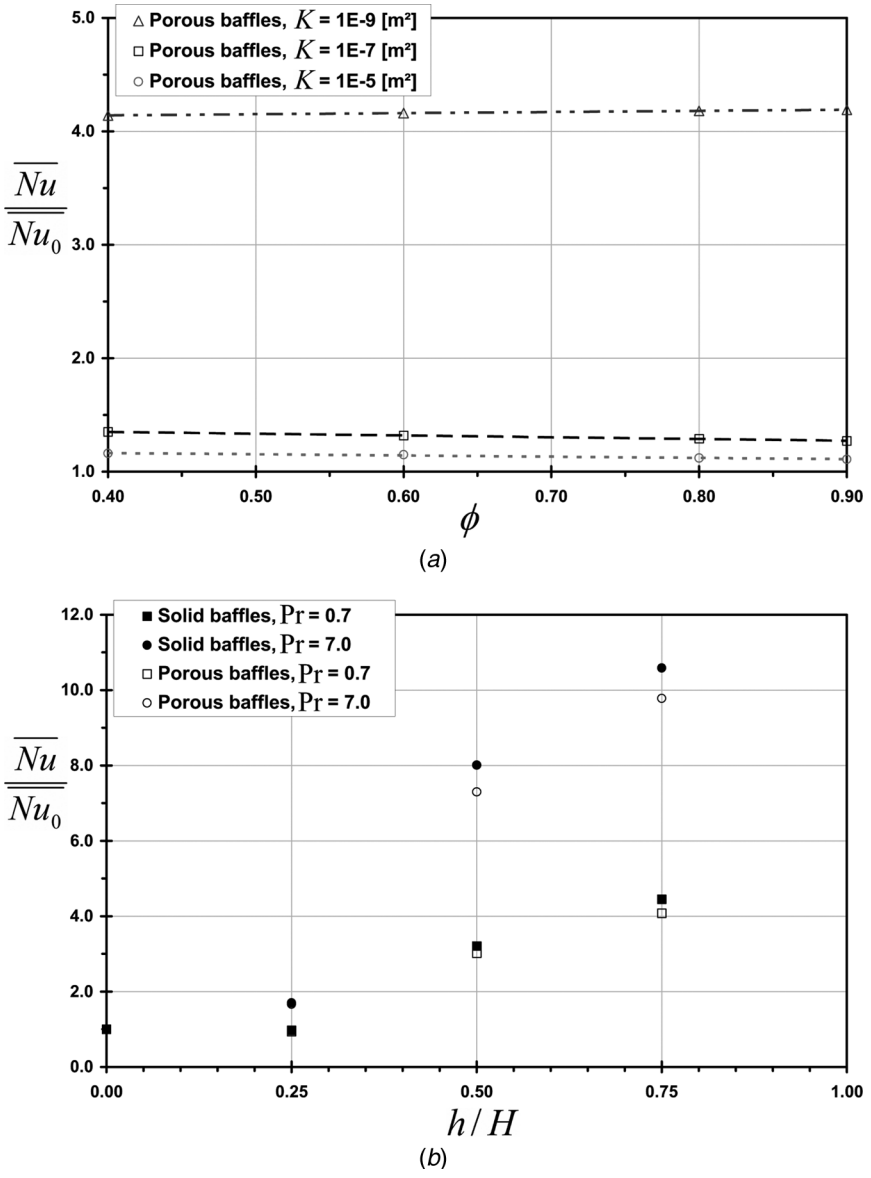

Figure 12. Nusselt number for a channel with baffles, $\lambda = 0.4$: (*a*) effect of ϕ, $h/H = 0.5$, $\mathrm{Pr} = 0.7$; (*b*) effect of h/H, $K = 1 \times 10^{-9}\,\mathrm{m}^2$, and $\phi = 0.4$.

Table 6 shows the effects of K and ϕ on $\overline{\mathrm{Nu}}^*$, covering a wide range of permeabilities, from $K = 10^{-9}\mathrm{m}^2$ to $10^{-5}\mathrm{m}^2$. The table indicates that porosity has a very weak influence on heat transfer characteristics for less permeable material, a result already shown in Figure 9*a* and Figure 12*a*. As the baffle becomes more permeable ($K = 10^{-5}\,\mathrm{m}^2$), then porosity starts to play a certain role on heat transfer performance, a result also seen in Figure 9*a* and Figure 12*a*. As expected, less permeable

Table 2. Effects of Re and Pr on $\overline{\mathrm{Nu}}^*$ for $h/H = 0.5$, $\lambda = 0.4$, $K = 1\times10^{-9}\,\mathrm{m}^2$, and $\phi = 0.40$

		$\overline{\mathrm{Nu}}^*$		
Re	Pr	Porous	Solid	η
100	0.7	0.57	0.59	−2.5%
300		0.68	0.71	−4.0%
500		0.76	0.80	−5.3%
100	7.0	1.11	1.21	−8.5%
300		1.64	1.77	−7.0%
500		1.95	2.12	−7.6%

Table 3. Effects of h/H and Pr on $\overline{\mathrm{Nu}}^*$ for $\mathrm{Re} = 300$, $\lambda = 0.4$, $K = 1\times10^{-9}\,\mathrm{m}^2$, and $\phi = 0.40$

		$\overline{\mathrm{Nu}}^*$		
h/H	Pr	Porous	Solid	η
0.25	0.7	0.57	0.59	−3.1%
0.5		0.68	0.71	−4.0%
0.75		0.63	0.65	−4.1%
0.25	7.0	1.01	1.03	−1.8%
0.5		1.64	1.77	−7.0%
0.75		1.50	1.55	−3.4%

Table 4. Effects of Pr and λ on $\overline{\mathrm{Nu}}^*$ for $h/H = 0.5$, $\mathrm{Re} = 300$, $K = 1\times10^{-9}\,\mathrm{m}^2$, and $\phi = 0.40$

		$\overline{\mathrm{Nu}}^*$		
Pr	λ	Porous	Solid	η
0.7	4.E −01	0.68	0.71	−4.0%
	4.E + 00	0.76	0.81	−5.8%
	4.E + 01	0.92	0.94	−2.7%
7.0	4.E −02	1.62	1.66	−2.3%
	4.E −01	1.64	1.77	−7.0%
	4.E + 00	1.79	1.85	−3.2%
	2.E + 01	2.10	2.14	−1.8%

baffles ($K = 10^{-9}\,\mathrm{m}^2$) tend to produce results for $\overline{\mathrm{Nu}}^*$ close to those using solid material. Finally, Table 7 indicates that for an increase in Re, the values of $\overline{\mathrm{Nu}}^*$ also rise for highly flow-resistant porous material ($K = 10^{-9}\,\mathrm{m}^2$) but, in turn, it decreases for lower values of K. High-Re flow across nearly solid porous baffles gives rise to strong recirculation motion, ultimately increasing ψ_0 (see Figure 6*a*). On the other hand, easier-to-flow porous baffles ($K = 1\times10^{-5}\,\mathrm{m}^2$) will let more fluid pass through the channel as Re increases, causing no recirculation motion and keeping $\psi_0 = 0$ (see Figure 6*c*).

In summary, none of the results above showed a situation where porous baffles presented better performance than the solid ones ($\eta > 0$). This, however, is in

Table 5. Effect on Re, λ, and ϕ on $\overline{\mathrm{Nu}}^*$ for $h/H = 0.5$, Pr = 0.7, and $K = 1 \times 10^{-9}\,\mathrm{m}^2$

		$\overline{\mathrm{Nu}}^*$				
		ϕ			η(ϕ)	
Re	λ	0.4	0.9	Solid	0.4	0.9
100		0.57	0.56	0.59	−2.5%	−3.8%
300	4.E − 01	0.68	0.68	0.71	−4.0%	−4.2%
500		0.76	0.76	0.80	−5.3%	−5.4%
100		0.76	0.69	0.76	0.0%	−9.0%
300	4.E + 01	0.92	0.81	0.94	−2.7%	−14.0%
500		1.05	0.90	1.07	−2.3%	−16.4%

Table 6. Effects on K and ϕ on $\overline{\mathrm{Nu}}^*$ for $h/H = 0.5$, Re = 500, Pr = 0.7, and λ = 0.4

		$\overline{\mathrm{Nu}}^*$			
ϕ	K [m^2]	1.0E − 09	1.0E − 07	1.0E − 05	Solid
0.4		0.76	0.41	0.74	0.80
0.6		0.76	0.40	0.71	
0.8		0.76	0.39	0.67	
0.9		0.76	0.39	0.66	

Table 7. Effects of Re, K, and ϕ on $\overline{\mathrm{Nu}}^*$ for $h/H = 0.5$, Pr = 0.7, and λ = 0.4

		$\overline{\mathrm{Nu}}^*$				
	K [m^2]	1.0E − 09	1.0E − 09	1.0E − 08	1.0E − 07	
Re	ϕ	0.4	0.9	0.9	0.9	Solid
100		0.57	0.56	0.55	0.50	0.59
200		0.63	—	—	—	0.65
300		0.68	0.68	0.52	0.41	0.71
400		0.72	—	—	—	0.76
500		0.76	0.76	0.42	0.39	0.80

agreement with results already presented in [9] and [43–45]. Nevertheless, for turbulent flow cases, advantages in using porous baffles might be possible, as already indicated in recent research efforts in the literature [6–8]. With such motivation, turbulent flow will be further investigated in this research program.

5. CONCLUSION

This work presented results for the numerical solution of laminar flow in a channel containing porous and solid (impermeable) obstructions. Discretization of the governing equations used the finite-volume method and a set of algebraic equations was solved by the SIMPLE method. The numerical results presented

for the friction factor f and for the Nusselt number Nu were compared with data of [2] and [4], indicating that results herein differ by less than 5% in relation to published results. Further simulations comparing the effectiveness of the porous material used showed that no advantages are obtained by using low-porosity and low-permeability baffles in the laminar flow regime. Finally, results herein are encouraging and motivate further analyses for simulating turbulent flow in porous-baffled channels.

REFERENCES

1. C. Berner, F. Dust, and D. M. McEligot, Flow Around Baffles, *J. Heat Transfer*, vol. 106, pp. 743–749, 1984.
2. K. M. Kelkar and S. V. Patankar, Numerical Prediction of Flow and Heat Transfer in a Parallel Plate Channel with Staggered Fins, *J. Heat Transfer*, vol. 109, pp. 25–30, 1987.
3. B. W. Webb and S. Ramadhyani, Conjugate Heat Transfer in a Channel with Staggered Ribs, *Int. J. Heat Mass Transfer*, vol. 28, no. 9, pp. 1679–1687, 1985.
4. J. R. Lopez, N. K. Anand, and L. S. Fletcher, Heat Transfer in a Three-Dimensional Channel with Baffles, *Numer. Heat Transfer A*, vol. 30, pp. 189–205, 1996.
5. P. C. Huang and K. Vafai, Internal Heat Transfer Augmentation in a Channel Using an Alternate Set of Porous Cavity-Block Obstacles, *Numer. Heat Transfer A*, vol. 25, no. 5, pp. 519–539, 1994.
6. J.-J. Hwang, Turbulent Heat Transfer and Fluid Flow in a Porous-Baffled Channel, *J. Thermophys. Heat Transfer*, vol. 11, no. 3, pp. 429–436, 1997.
7. Y.-T. Yang and C.-Z. Hwang, Calculation of Turbulent Flow and Heat Transfer in a Porous-Baffled Channel, *Int. J. Heat Transfer*, vol. 46, pp. 771–780, 2003.
8. Kang-Hoon Ko and N. K. Anand, Use of Porous Baffles to Enhance Heat Transfer in a Rectangular Channel, *Int. J. Heat Mass Transfer*, vol. 46, pp. 4191–4199, 2003.
9. B. M. Da Silva Miranda and N. K. Anand, Convective Heat Transfer in a Channel with Porous Baffles, *Numer. Heat Transfer A*, vol. 46, no. 5, pp. 425–452, 2004.
10. A. Haji-Sheikh, W. J. Minkowycz, and E. M. Sparrow, A Numerical Study of the Heat Transfer to Fluid Flow through Circular Porous Passages, *Numer. Heat Transfer A*, vol. 46, no. 10, pp. 929–955, 2004.
11. F. D. Rocamora, Jr. and M. J. S. de Lemos, Prediction of Velocity and Temperature Profiles for Hybrid Porous Medium-Clear Fluid Domains, *Proc. CONEM2000—National Mechanical Engineering Congress* (on CD-ROM), Natal, Rio Grande do Norte, Brazil, August 7–11, 2000.
12. F. D. Rocamora, Jr. and M. J. S. de Lemos, Laminar Recirculating Flow and Transfer in Hybrid Porous Medium—Clear Fluid Computational Domains, *Proc. 34th ASME Natl. Heat Transfer Conf.* (on CD-ROM), Pittsburgh, PA, August 20–22, 2000, ASME-HTD-1463CD, Paper NHT2000-12317.
13. J. A. Ochoa-Tapia and S. Whitaker, Momentum Transfer at the Boundary between a Porous Medium and a Homogeneous Fluid—II: Comparison with Experiment, *Int. J. Heat Mass Transfer*, vol. 38, pp. 2647–2655, 1995.
14. J. A. Ochoa-Tapia and S. Whitaker, Momentum Transfer at the Boundary between a Porous Medium and a Homogeneous Fluid—I: Theoretical Development, *Int. J. Heat Mass Transfer*, vol. 38, pp. 2635–2646, 1995.
15. A. V. Kuznetsov, Analytical Investigation of the Fluid Flow in the Interface Region between a Porous Medium and a Clear Fluid in Channels Partially with a Porous Medium, *Appl. Sci. Res.*, vol. 56, pp. 53–56, 1996.

16. A. V. Kuznetsov, Influence of the Stress Jump Condition at the Porous-Medium/Clear-Fluid Interface on a Flow at a Porous Wall, *Int. Commun. Heat Mass Transfer*, vol. 24, pp. 401–410, 1997.
17. A. V. Kuznetsov, Fluid Mechanics and Transfer in the Interface Region between a Porous Medium and a Fluid Layer: A Boundary Layer Solution, *J. Porous Media*, vol. 2, no. 3, pp. 309–321, 1999.
18. A. V. Kuznetsov, L. Cheng, and M. Xiong, Effects of Thermal Dispersion and Turbulence in Forced Convection in a Composite Parallel-Plate Channel: Investigation of Constant Wall Heat Flux and Constant Wall Temperature Cases, *Numer. Heat Transfer A*, vol. 42, no. 4, pp. 365–383, 2002.
19. R. A. Silva and M. J. S. de Lemos, Numerical Treatment of the Stress Jump Interface Condition for Laminar Flow in a Channel Containing a Porous Layer, *Numer. Heat Transfer A*, vol. 43, no. 6, pp. 603–617, 2003.
20. L. A. Tofaneli and M. J. S. de Lemos, Escoamento Laminar em Região Espacialmente Periódica em Canal Contendo Obstrução Porosa (in Portuguese), *Proc. CONEM2002—National Mechanical Engineering Congress*, João Pessoa, Brazil, August 12–16, 2002, Paper CPB0275.
21. L. A. Tofaneli and M. J. S. de Lemos, Influência da Porosidade e da Permeabilidade de Aletas Porosas no Escoamento em Regime Laminar em Canal Entre Placas (in Portuguese), *Proc. ENCIT2002—National Thermal Sciences Meeting*, Caxambú, Brazil, October 13–17, 2002.
22. M. J. S. de Lemos and L. A. Tofaneli, Application of a Macroscopic Turbulence Model to Simulation of Flow in a Channel with Equally Spaced Porous Fins, *Proc. ASME Summer Heat Transfer Conf.* (on CD-ROM), Las Vegas, NV, July 21–23, 2003, Paper HT 2003-40248.
23. M. J. S. de Lemos and L. A. Tofaneli, Pressure Drop Characteristics of Parallel-Plate Channel Flow with Porous Obstructions at Both Walls, *Proc. 2003 ASME International Mechanical Engineering Congress* (on CDROM), Washington, DC, November 16–21, 2003, Paper IMECE2003-41453.
24. M. H. J. Pedras and M. J. S. de Lemos, On the Definition of Turbulent Kinetic Energy for Flow in Porous Media, *Int. Commun. Heat Mass Transfer*, vol. 27, no. 2, pp. 211–220, 2000.
25. M. H. J. Pedras and M. J. S. de Lemos, Macroscopic Turbulence Modeling for Incompressible Flow through Undeformable Porous Media, *Int. J. Heat Transfer*, vol. 44, no. 6, pp. 1081–1093, 2001.
26. M. H. J. Pedras and M. J. S. de Lemos, Simulation of Turbulent Flow in Porous Media Using a Spatially Periodic Array and a Low Re Two-Equation Closure, *Numer. Heat Transfer A*, vol. 39, no. 1, pp. 35–59, 2001.
27. M. H. J. Pedras and M. J. S. de Lemos, On the Mathematical Description and Simulation of Turbulent Flow in a Porous Medium Formed by an Array of Elliptic Rods, *J. Fluids Eng.*, vol. 123, no. 4, pp. 941–947, 2001.
28. M. H. J. Pedras and M. J. S. de Lemos, Computation of Turbulent Flow in Porous Media Using a Low Reynolds $k-\varepsilon$ Model and an Infinite Array of Transversally Displaced Elliptic Rods, *Numer. Heat Transfer A*, vol. 43, no. 6, pp. 585–602, 2003.
29. F. D. Rocamora, Jr. and M. J. S. de Lemos, Analysis of Convective Heat Transfer of Turbulent Flow in Saturated Porous Media, *Int. Commun. Heat Mass Transfer*, vol. 27, no. 6, pp. 825–834, 2000.
30. M. J. S. de Lemos and F. D. Rocamora, Turbulent Transport Modeling for Heated Flow in Rigid Porous Media, *Proc. Twelfth Int. Heat Transfer Conf.*, Grenoble, France, August 18–23, 2002, pp. 791–795.
31. M. J. S. de Lemos and E. J. Braga, Modeling of Turbulent Natural Convection in Saturated Rigid Porous Media, *Int. Commun. Heat Mass Transfer*, vol. 30, no. 5, pp. 615–624, 2003.

32. E. J. Braga and M. J. S. de Lemos, Turbulent Natural Convection in a Porous Square Cavity Computed with a Macroscopic k–ε Model, *Int. J. Heat Mass Transfer*, vol. 47, no. 26, pp. 5635–5646, 2004.
33. E. J. Braga and M. J. S. de Lemos, Heat Transfer in Enclosures Having a Fixed Amount of Solid Material Simulated with Homogeneous and Heterogeneous Models, *Int. J. Heat Mass Transfer*, in press, 2005.
34. M. J. S. de Lemos and M. S. Mesquita, Turbulent Mass Transport in Saturated Rigid Porous Media, *Int. Commun. Heat Mass Transfer*, vol. 30, no 1, pp. 105–113, 2003.
35. M. Saito and M. J. S. de Lemos, Interfacial Heat Transfer Coefficient for Non-Equilibrium Convective Transport in Porous Media, *Int. Commun. Heat Mass Transfer*, vol. 32, no. 5, pp. 667–677, 2005.
36. M. J. S. de Lemos and L. A. Tofaneli, Modeling of Double-Diffusive Turbulent Natural Convection in Porous Media, *Int. J. Heat Mass Transfer*, vol. 47, no. 19–20, pp. 4233–4241, 2004.
37. M. J. S. de Lemos and M. H. J. Pedras, Modeling Turbulence Phenomena in Incompressible Flow through Saturated Porous Media, *Proc. 34th ASME Natl. Heat Transfer Conf.* (on CD-ROM), Pittsburgh, PA, August 20–22, 2000, ASME-HTD-I463CD, Paper NHTC2000-12120.
38. M. J. S. de Lemos and M. H. J. Pedras, Simulation of Turbulent Flow through Hybrid Porous Medium Clear Fluid Domains, *Proc. IMECE2000 ASME Int. Mechanical Engineering Congress*, Orlando, FL, November 5–10, 2000, ASME-HTD-366-5, pp. 113–122.
39. R. A. Silva and M. J. S. de Lemos, Turbulent Flow in a Channel Occupied by a Porous Layer Considering the Stress Jump at the Interface, *Int. J. Heat Mass Transfer*, vol. 46, no. 26, pp. 5113–5121, 2003.
40. M. J. S. de Lemos, Turbulent Kinetic Energy Distribution across the Interface between a Porous Medium and a Clear Region, *Int. Commun. Heat Mass Transfer*, vol. 32, nos. 1–2, pp. 107–115, 2005.
41. A. M. Assato, M. H. J. Pedras, and M. J. S. de Lemos, Numerical Solution of Turbulent Flow past a Backward-Facing-Step with a Porous Insert Using Linear and Non-linear $k-\varepsilon$ Models, *J. Porous Media*, vol. 8, no. 1, pp. 13–29, 2005.
42. M. J. S. de Lemos and M. H. J. Pedras, Recent Mathematical Models for Turbulent Flow in Saturated Rigid Porous Media, *J. Fluids Eng.*, vol. 123, no. 4, pp. 935–940, 2001.
43. N. B. Santos and M. J. S. de Lemos, Laminar Flow and Heat Transfer Analysis in a Channel with Porous Baffles, *Proc. CONEM2004—Natl. Mechanical Engineering Congress* (on CD-ROM), Belém, Brazil, August 10–13, 2004.
44. M. J. S. de Lemos and N. B. Santos, Laminar Heat Transfer in a Parallel Plate Channel with Solid and Porous Baffles, *Proc. IMECE04—2004 ASME Int. Mechanical Engineering Congress*, Anaheim, CA, November 13–20, 2004, Paper IMECE2004-62362.
45. N. B. Santos and M. J. S. de Lemos, Effect of Porosity and Permeability on Heat Transfer Enhancement in Channels with Porous Baffles, *Proc. ENCIT 2004—Natl. Thermal Sciences Meeting* (on CD-ROM), Rio de Janeiro, Brazil, November 29–December 3, 2004.
46. S. V. Patankar, *Numerical Heat Transfer and Fluid Flow*, Hemisphere, New York, 1980.